Research Square

Preprints are preliminary reports that have not undergone peer review.
They should not be considered conclusive, used to inform clinical practice,
or referenced by the media as validated information.

Cross-Shore Profile Symmetry and Hydrodynamic Exposure Adjacent to Maritime Structures

Filipe de Oliveira Santana
Federal University of South Bahia
Marcelo Soares Teles Santos
Federal University of South Bahia
Francisco de Deus Fonseca Neto
Federal Institute of Espírito Santo
Maria Carolina Hernandez Ribeiro
State University of Campinas
Eduardo Siegle
University of São Paulo
Anderson Targino da Silva Ferreira
andersontsferreira@usp.br

University of São Paulo

Research Article

Keywords: Coastal geomorphology, GNSS/RTK, Digital Elevation Model – DEM, Beach morphodynamics, Coastal engineering

Posted Date: November 18th, 2026

DOI: https://doi.org/10.21203/rs.3.rs-11578438/v1

License: This work is licensed under a Creative Commons Attribution 4.0 International License.
Read Full License

Additional Declarations: No competing interests reported.

Cross-Shore Profile Symmetry and Hydrodynamic Exposure Adjacent to Maritime Structures

Filipe de Oliveira Santos [1], Marcelo Soares Teles Santos [1], Francisco de Deus Fonseca Neto [2], Maria Carolina Hernandez Ribeiro [3], Eduardo Siegle [4], Anderson Targino da Silva Ferreira [4,5,6,*]

[1] Federal University of Southern Bahia, Itabuna 45600-923, Brazil.
[2] Federal Institute of Espírito Santo, Vitória, 29040-780, Brazil.
[3] Faculty of Agricultural Engineering, State University of Campinas, Campinas, Brazil.
[4] Oceanographic Institute, University of São Paulo, São Paulo 05508-120, Brazil.
[5] Federal University of ABC, Center for Natural and Human Sciences, São Bernardo do Campo, 09606-045, Brazil.
[6] Institute of Geosciences, State University of Campinas, Campinas 13083-855, Brazil.

[*] Author correspondence: andersontsferreira@usp.br

Abstract: Coastal infrastructure can alter nearshore hydrodynamic and sedimentary processes, yet rapid diagnostic assessments often lack high-accuracy geometric baselines. This study evaluates integrating geodetic GNSS/RTK surveying, high-resolution Digital Elevation Models (DEMs), and numerical wave reanalysis (WAVEWATCH III) to assess beach morphometry and hydrodynamic exposure adjacent to the Malhado International Port in Ilhéus, Brazil. Independent vertical accuracy assessment confirmed that the generated DEMs met Class A 1:1,000 cartographic standards (RMSE < 0.15 m). Multivariate and univariate analyses of variance (MANOVA/ANOVA) across eight morphodynamic parameters revealed no statistically significant differences ($p > 0.30$) between the updrift and downdrift beach sectors under modal eastward wave forcing. These results indicate homogeneous cross-shore geometric responses during the surveyed epoch, underscoring that detecting persistent sediment deficit requires multitemporal monitoring. This geodetic framework provides an objective tool to support coastal management and Sustainable Development Goals 14, 11, and 13.

Keywords: Coastal geomorphology; GNSS/RTK; Digital Elevation Model – DEM; Beach morphodynamics; Coastal engineering.

1. Introduction

Sandy beaches are dynamic environments whose morphology results from the interaction between waves, currents, tides, winds, sediment characteristics, and coastal geological configuration. These factors control sediment transport and redistribution, while changes in beach shape also influence local hydrodynamics. The interaction between processes and landforms produces spatial and temporal variations in beach profiles and the shoreline (Calliari et al., 2003; Castelle and Masselink, 2023; Wright and Short, 1984). Beach surface elevation, shoreline position, and profile width and slope describe the configuration and allow comparison of beach sections. However, a single observation characterizes conditions only at the time of the survey; identifying trends of erosion, accretion, or stability requires repeated surveys or multitemporal datasets. This distinction matters because observed changes may reflect both natural drivers, such as sea-level variations and extreme events, and human pressures (Cooley et al., 2022). Multitemporal monitoring using geotechnologies enables tracking these changes and supports coastal planning (Cabral, 2025).

Urbanization and engineering interventions can modify coastal dynamics by altering circulation, sediment availability, and the use of environments such as dunes and *restingas* (coastal vegetation zones). Ports, jetties, groins, and breakwaters can interrupt or redirect longshore transport, promoting sediment accumulation on the updrift side and reducing supply to the downdrift side. However, these effects vary depending on the direction of predominant drift, wave regime, sediment supply, coastal orientation and configuration, and the characteristics of the structure; therefore, they do not constitute universal responses (Bittencourt et al., 2005; Franzen et al., 2026, 2021; Saengsupavanich et al., 2024).

Coastal erosion and accretion also result from interactions among natural processes, human occupation, and climate change. Along Brazil's northeastern coast, responses vary across stretches, while global analyses map the spatial distribution of erosion and accretion. Sea-level rise and extreme events can exacerbate coastal risks, yet attributing changes to a specific factor requires consideration of local conditions (A. T. Ferreira et al., 2014; Gaya et al., 2022; Guerra et al., 2025; Mentaschi et al., 2018; Santos and Amaro, 2013). Port-related coastal structures, such as breakwaters and jetties, can alter wave propagation and local current patterns and interrupt or redirect longshore sediment transport (Gallerano et al., 2020; Tang et al., 2017). Field studies also document changes in beach erosion and deposition near ports where breakwaters obstruct sediment transport (A. T. Ferreira et al., 2014; Santos and Amaro, 2013; Uda and Yamamoto, 1994).

Understanding beach morphodynamics requires considering the interactions among waves, currents, tides, sediments, and coastal configuration (Calliari et al., 2003; Short, 1999; Wright and Short, 1984). Beach morphometry, characterized by elevation and slope, can be linked to dissipative, intermediate, and reflective states.

Together with shoreline orientation (aspect) and the wave climate, these attributes help interpret sediment transport and deposition patterns associated with port structures (Bujan et al., 2019; A. T. da S. Ferreira et al., 2024; Ferreira et al., 2025b, 2025a, 2023, 2021; A. T. S. Ferreira et al., 2024; Taveira-Pinto et al., 2022).

In this context, this study investigates how beach morphometry analysis, alongside oceanographic data, can help interpret the morphodynamic conditions of coastal areas with engineering structures. It aims to determine whether contrasts in elevation, shoreline position, width, and slope can indicate patterns of sediment redistribution and potential susceptibility to erosion, even in seemingly stable sectors. This perspective can enable faster assessments without continuous monitoring, although it does not, on its own, establish temporal trends or causal relationships. By providing information that supports the sustainable management of coastal ecosystems and resilient planning, this work offers a potential contribution to Sustainable Development Goal (SDG) 14, specifically Target 14.2, and, complementarily, to SDGs 11 (Target 11.b) and 13 (Target 13.1) (United Nations, 2020, 2015).

2. Methodological approach

2.1. Study area

The study area is located in Trincheiras Cove, adjacent to the Malhado International Port in the municipality of Ilhéus, on the southern coast of Bahia, Brazil (Figure 1). The port was inaugurated in 1971 to replace the old port at Pontal Bay, where channel siltation limited access for larger vessels. Its construction was linked to modernizing regional transport for production, historically associated with cocoa farming (Santos, 2016).

The region's meteoceanographic conditions vary seasonally. Along the Bahia coast, northeasterly and easterly winds dominate in spring and summer, whereas southeasterly and easterly winds, along with episodes associated with cold-front passages, characterize autumn and winter. These shifts influence wave incidence direction and sediment dispersion along the coast (Bittencourt et al., 2000). For the waters off Ilhéus, an analysis of WAVEWATCH III model reanalysis data (1979–2009) identified predominant waves from the east and southeast, mean periods under 10 seconds, and peak energy between June and September. Modeled wave heights ranged from 0.39 to 4.89 m; these values represent estimated offshore conditions rather than specific measurements taken near the beaches or the port (Lobo et al., 2017; Pianca et al., 2010).

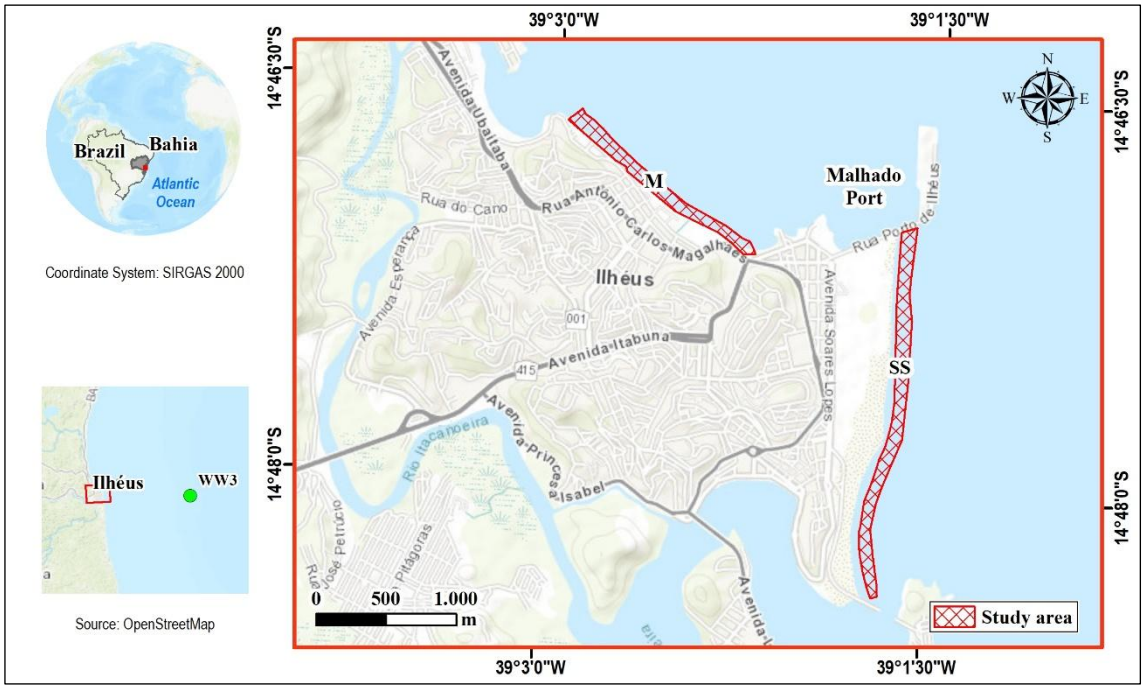


Figure 1. Study areas in Ilhéus, Bahia: M (Malhado), north of the Malhado International Port, and SS (São Sebastião), south of the port. The green dot indicates the offshore position associated with the WAVEWATCH III (WW3) model. Coordinate system: SIRGAS 2000. Base map: OpenStreetMap.

2.2. GNSS/RTK position

Topographic data were collected on foot using CHC i90 dual-frequency GNSS receivers operating in RTK mode. The method uses phase observations and resolves integer ambiguities to obtain three-dimensional coordinates with centimeter-level precision, depending on solution quality and observation conditions (Halaj and Kačmařík, 2022; Hofmann-Wellenhof et al., 2008; Krueger et al., 2020; Monico, 2008; Santos et al., 2013). For baselines of up to 10 km, the stated nominal precision is 8 mm + 1 ppm horizontally and 15 mm + 1 ppm vertically.

Approximately 2.5 km were traversed in each sector, at São Sebastião Beach (up-drift) and Malhado Beach (down-drift of the port), recording beach features along south–north paths. The pole was held vertically at 2 m. Data collection took place near spring low tide, within the one-hour window before and after the Brazilian Navy's predicted time. The coastline was represented by the altitude isoline normal to 0 m, extracted from the altimetric data. The geometric altitudes were converted to normal altitudes using the hgeoHNOR2020 model at the Brazilian Institute of Geography and Statistics (IBGE) (Equation 1). While the uncertainty (Equation 2) was estimated via variance propagation, assuming independent errors (Ferreira et al., 2024; Ferreira et al., 2024; Santos et al., 2013).

$$H = h - N \quad (1)$$

$$s_H = \sqrt{s_h^2 + s_N^2} \quad (2)$$

2.3. Digital elevation model (DEM)

The Digital Elevation Models (DEMs) were generated via linear interpolation within an Irregular Triangular Network (TIN), connecting sample points into contiguous triangles without extrapolation beyond the sampling domain. The mesh was constructed using the Delaunay algorithm, based on the circumcircle criterion, which maximizes minimum internal angles and avoids excessively thin or acute triangles (A. T. Ferreira et al., 2014; Ferreira et al., 2021, 2019, 2016; A. T. S. Ferreira et al., 2024; Santos et al., 2013; Sofia et al., 2019).

Positional validation followed the Technical Specification Standard for Geospatial Data Quality Control (ET-CQDG), which establishes positional accuracy standards for digital cartographic products. Altimetric discrepancies $e_{z,i}$ were determined using independent Check Points (CP) obtained via GNSS/RTK receivers:

$$e_{z,i} = Z_{t,i} - Z_{r,i} \quad (3)$$

Where $Z_{t,i}$ represents the elevation estimated by the DEM and $Z_{r,i}$ the reference altitude at point i. Global dispersion was quantified by the Root Mean Square Error (RMSE):

$$RMSE = \sqrt{\frac{1}{n}\sum_{i=1}^{n} e_{z,i}^2} \quad (4)$$

Let n be the sample size of checkpoints (CP). Model conformity requires simultaneously meeting two normative statistical thresholds: at least 90% of the absolute discrepancies ($e_{z,i}$) must be less than or equal to the Maximum Error (ME), and the calculated RMSE must not exceed the Standard Error (SE) stipulated for the tested class (A, B, C, or D) and scale.

2.4. Oceanographic wave parameters and strandline altitude (SA)

The wave regime is characterized using hourly output from the global WAVEWATCH III (WW3) model, distributed by the Pacific Islands Ocean Observing System (PacIOOS). A Python script (https://doi.org/10.5281/zenodo.23369947) processes the grid point located at −14.795231° latitude and −38.838319° longitude and extracts significant wave height (Hs), peak period (Tp), and peak direction (Dp), together with swell and wind-wave height, period, and direction when available. Assuming a narrow-band Rayleigh distribution, the script estimates wave heights associated with exceedance probabilities and the probable maximum wave height, including H_2%, the height exceeded by 2% of waves (Ferreira et al., 2024; Holthuijsen, 2007; Tolman et al., 2002).

Strandline altitude (SA) is calculated as the sum of wave run-up (Wr) and maximum tidal elevation (Th), both referenced to a fixed vertical datum. Wave run-up is estimated with the Stockdon et al. (2006) parameterization, using the WW3 significant wave height as offshore significant wave height (H_0):

$$W_r = 1.1\left((0.35\beta(H_0L_0)^{0.5} + \frac{[H_0L_0\,(0.563\beta^2 + 0.004)]^2}{2}\right) \quad (5)$$

Here, H_0 is offshore significant wave height, L_0 is offshore wavelength, and β is the beach-face slope in radians. The formulation assumes normally incident waves; refraction can cause oblique incidence and may overestimate run-up (Stein & Siegle, 2020). Foreshore sediment size can also affect infiltration, swash-flow asymmetry, and beach slope (Andrade et al., 2019; Bujan et al., 2019). SA is then obtained as:

$$S_A = W_r + T_h \quad (6)$$

SA values are classified relative to their mean (μ) and standard deviation (σ): very low (< μ − 2σ), low (μ − 2σ to μ − σ), medium (μ − σ to μ + σ), high (μ + σ to μ + 2σ), and very high (> μ + 2σ). The very-high class represents the storm-water level associated with the positive combination of storm surge and astronomical tide (Ferreira et al., 2024).

2.5. Multivariate statistical analysis

Multivariate analysis of variance (MANOVA) was used to assess differences between the mean vectors of the profile characteristics of the two beach sectors adjacent to Malhado Port (Rencher and Christensen, 2012; Timm, 2002). The sectors comprised Malhado Beach (M), north of the port, and São Sebastião Beach (SS), south of the port, with 16 profiles surveyed in each sector. Eight profile-level variables were included: number of survey points (N_points), first-point elevation (H_first_m), last-point elevation (H_last_m), elevation difference between

the first and last points (dH_m), horizontal profile length (Hdist_m), beach-face slope (tan_beta), estimated wave run-up (Wr_m), and estimated strandline altitude (SA_m). Beach sector was the grouping factor.

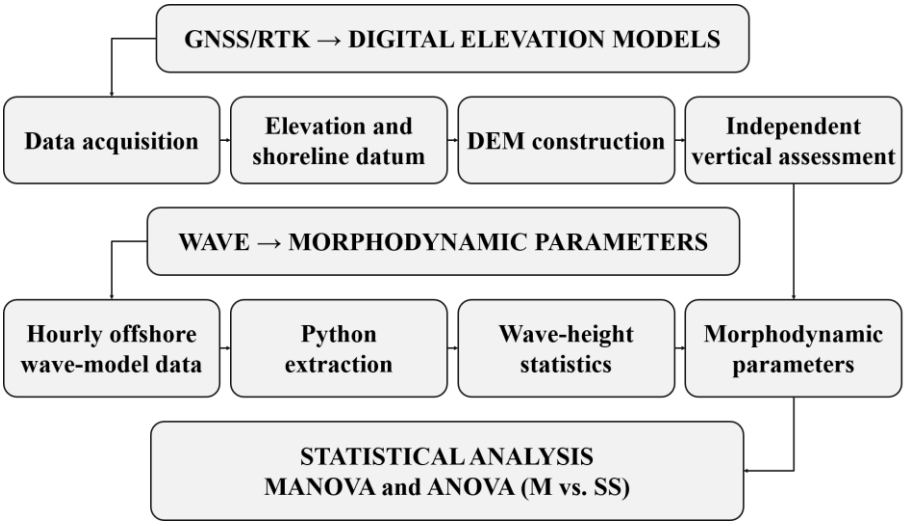


Figure 2. Methodological workflow integrating GNSS/RTK surveys, digital elevation model (DEM) generation and independent vertical accuracy assessment, offshore wave-model data processing, morphodynamic parameter estimation, and statistical comparison between Malhado (M) and São Sebastião (SS) beaches using MANOVA and ANOVA, in Ilhéus, Bahia, Brazil.

3. Results

3.1. DEM generation and accuracy assessment

The DEMs depict contrasting altimetric ranges between the two beach sectors. SS ranges from −2.377 to 1.170 m (3.547 m), whereas M ranges from −2.149 to 0.611 m (2.760 m); the difference between these ranges is 0.787 m. The Tanβ maps show spatially heterogeneous slopes along both shorelines. The mean slope β is slightly higher at SS (0.026810) than at M (0.026039), and its standard deviation is also higher at SS (0.017154 versus 0.013607). However, the maximum value is higher at M (0.083238) than at SS (0.075763) (Figure 3). These patterns characterize the surveyed relief and slope distribution but, by themselves, do not demonstrate sediment accumulation, erosion, or geomorphological stability. Independent check-point assessment yields RMSE values of 0.144 m for SS and 0.119 m for M, both below the 0.167 m standard-error limit. At both beaches, 100% of discrepancies are below the 0.270 m maximum-error limit. Accordingly, both DEMs meet the altimetric criteria for Class A at 1:1,000 under PAP-PCD/ET-CQDG (Table 1).

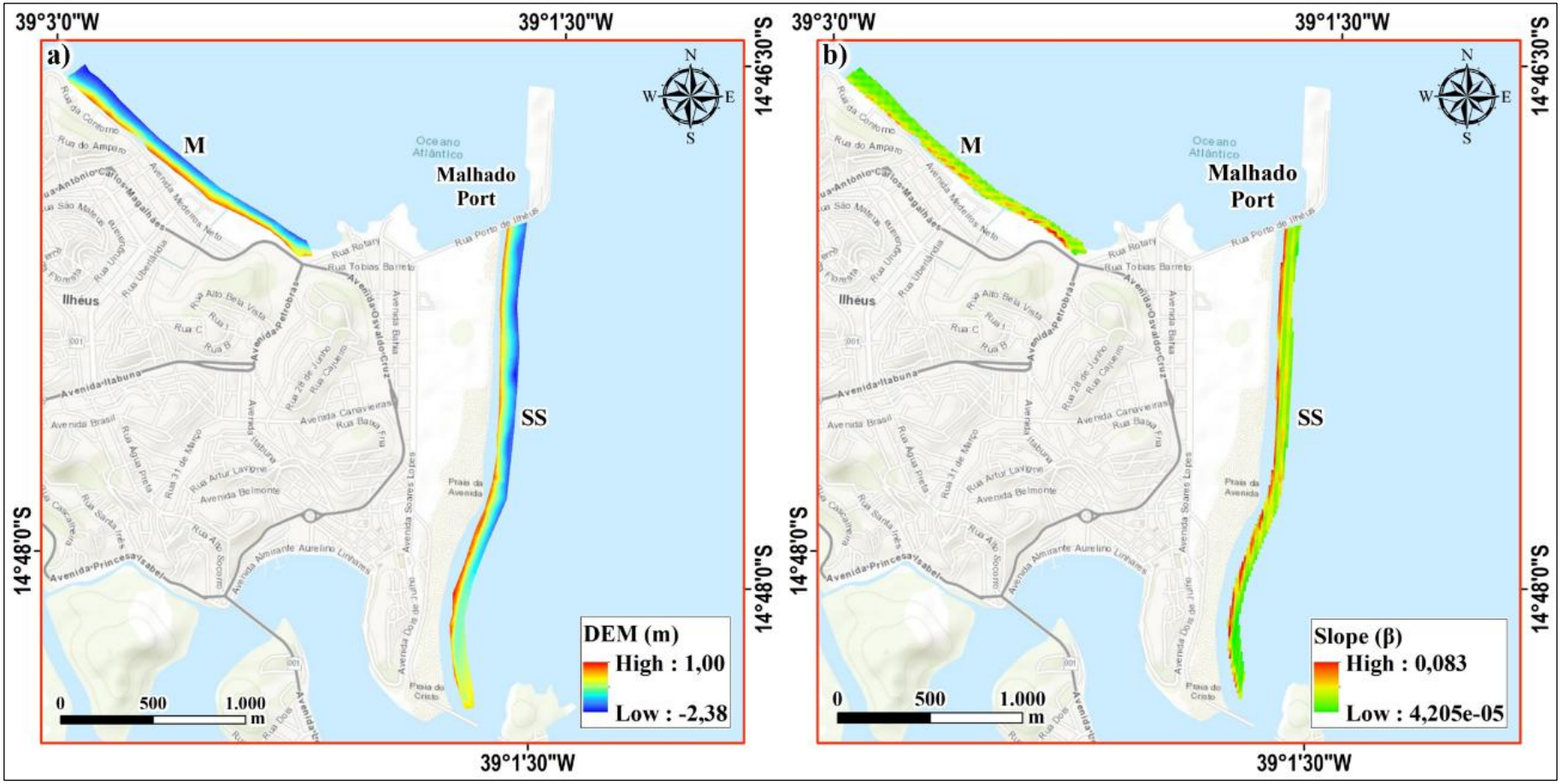


Figure 3. Spatial distribution of (a) digital elevation and (b) beach slope (β) along Malhado (M) and São Sebastião (SS) beaches, north and south of Malhado Port, respectively, in Ilhéus, Bahia, Brazil.

Tabela 1. GNSS/RTK precision statistics for DEM sample points and check points (CP), with DEM elevation and vertical-accuracy results. n = number of points; precision triplets are easting (sE)/northing (sN)/height (sh), in meters. Discrepancies compare GNSS/RTK reference and DEM-derived elevations; CP percentage is the share below the maximum-error limit. Class A at 1:1,000: standard-error limit = 0.167 m; maximum-error limit = 0.270 m. SS = São Sebastião; M = Malhado; RMSE = root mean square error; PAP-PCD reports class and scale; — = not applicable.

Statistic or parameter	Sample points (n = 453)	SS CP (n = 10)	M CP (n = 10)	SS DEM	M DEM
Number of points	453	10	10	—	—
Mean precision (m)	0.009 / 0.009 / 0.023	0.009 / 0.005 / 0.022	0.008 / 0.009 / 0.022	—	—
Precision standard deviation (m)	0.002 / 0.002 / 0.004	0.005 / 0.005 / 0.006	0.001 / 0.001 / 0.001	—	—
Minimum precision (m)	0.007 / 0.007 / 0.016	0.007 / 0.007 / 0.016	0.007 / 0.008 / 0.020	—	—
Maximum precision (m)	0.028 / 0.027 / 0.076	0.025 / 0.024 / 0.065	0.009 / 0.011 / 0.023	—	—
Precision range (m)	0.035 / 0.034 / 0.092	0.018 / 0.017 / 0.049	0.002 / 0.003 / 0.003	—	—
Minimum elevation (m)	—	—	—	−2.377	−2.149
Maximum elevation (m)	—	—	—	1.170	0.611
Altimetric range (m)	—	—	—	3.547	2.760
Mean discrepancy (m)	—	—	—	−0.001	0.067
Discrepancy standard deviation (m)	—	—	—	0.127	0.078
Root mean square error (RMSE, m)	—	—	—	0.144	0.119
Permissible standard error, Class A at 1:1,000 (m)	—	—	—	0.167	0.167
CPs below the 0.270 m maximum error	—	—	—	100%	100%
PAP-PCD classification	—	—	—	Class A, 1:1,000	Class A, 1:1,000

3.2. Morphometric, morphodynamic, and metoceanographic parameters

The wave time series for the displayed period (2017–2025) shows substantial temporal fluctuations in significant wave height (Hs), H_2%, maximum wave height (Hmax), and peak period (Tp). Hs generally varies between approximately 0.7 and 2.0 m, with episodic peaks near 2.5 m. H_2% reaches approximately 3.8 m, while Hmax approaches 5.0 m. Tp most frequently ranges from 6 to 10 s, although occasional values exceed 15 s (Figure 4a). The directional distribution is strongly concentrated around east (approximately 90°), with a secondary concentration toward east-northeast (Figure 4b).

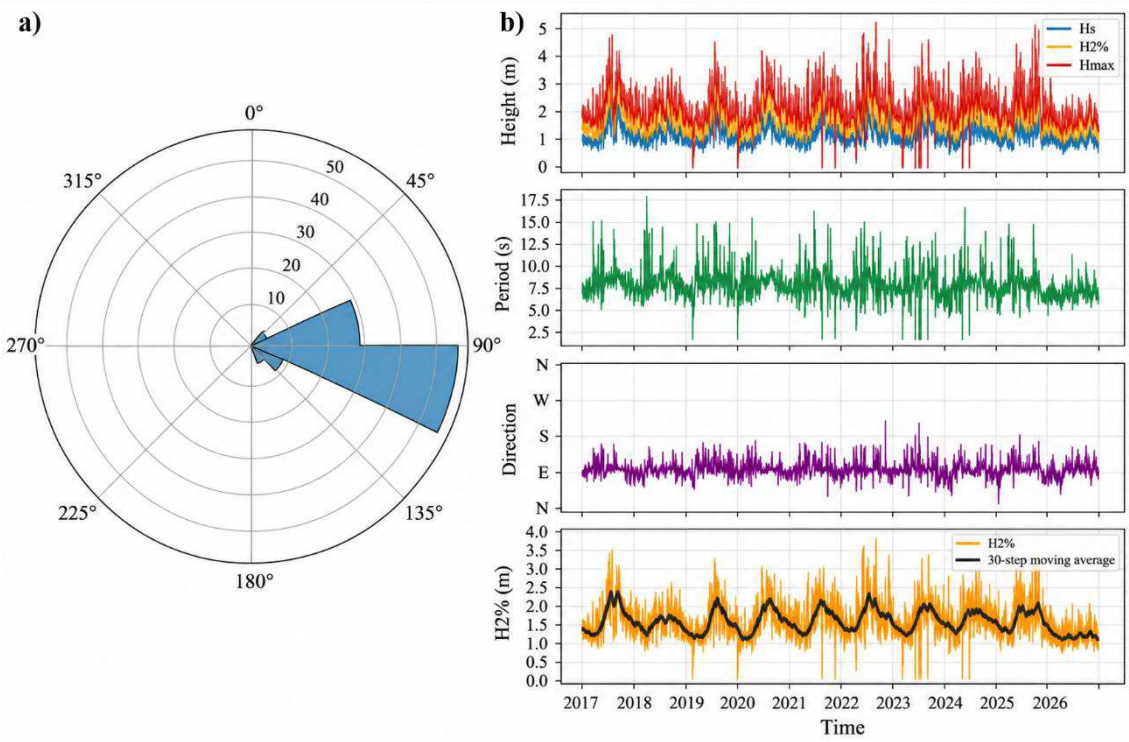


Figure 4. Characterization of the wave regime in Ilhéus, Bahia: (a) wave rose, showing the percentage distribution of waves; (b) time series of significant wave height (Hs), wave height exceeded by 2% of waves (H2%), maximum wave height (Hmax), peak period (Tp), and wave direction. The bottom panel shows H2% and its 30-day moving average.

Table 2 summarizes 32 beach profiles, with 16 surveyed at each beach. The number of observations per profile ranges from 11 to 25 at M and from 7 to 34 at SS. The elevation difference (dH) is negative across all M profiles (−2.3518 to −0.2483 m); at SS, it ranges from −2.6577 to 0.0597 m, with SS01 recording the only positive value. Profile distances range from 60.8428 to 124.7550 m at M and from 49.9114 to 109.1864 m at SS. The tangent of the beach-face slope (tan β) ranges from −0.0359 to −0.0040 at M and from −0.0326 to 0.0012 at SS. Mean first-point elevations are 0.1448 m at M and 0.4176 m at SS; mean last-point elevations are −1.5605 and −1.3202 m. Mean slope angles are −1.2108° (−0.0211 rad) at M and −1.1426° (−0.0199 rad) at SS. Wave run-up (Wr) ranges from 0.5662 to 0.7856 m at M and from 0.5839 to 0.8318 m at SS; strandline altitude (SA) ranges from 2.5662 to 2.7856 m at M and from 2.5839 to 2.8318 m at SS. Each beach has 10 intermediate and 6 dissipative profiles. The medium SA class occurs in 12 profiles per beach; the remaining profiles are classified as low (one per beach), high (three at M and two at SS), or very high (one at SS).

Tabela 2. Beach-profile parameters and classifications for Malhado (M) and São Sebastião (SS): *N_points*, number of survey points; *H_first_m* and *H_last_m*, first and last profile elevations; *dH_m*, elevation difference; *Hdist_m*, horizontal profile distance; *tan_beta*, slope tangent; *beta_deg* and *beta_rad*, slope in degrees and radians; *Wr_m*, wave run-up; *SA_m*, strandline altitude. Elevations, distances, *Wr*, and *SA* are in meters.

Profile	N_points	H_first_m	H_last_m	dH_m	Hdist_m	tan_beta	beta_deg	beta_rad	Wr_m	SA_m	Morpho_state	SA_class
M01	13	0.0419	-1.8273	-1.8692	83.2671	-0.0224	-1.2860	-0.0224	0.6455	2.6455	Intermediate	Medium
M02	14	0.3327	-1.8255	-2.1583	75.8482	-0.0285	-1.6299	-0.0284	0.6079	2.6079	Intermediate	Medium
M03	15	0.4378	-1.7450	-2.1829	60.8428	-0.0359	-2.0547	-0.0359	0.5662	2.5662	Intermediate	Low
M04	13	0.4234	0.1750	-0.2483	62.4418	-0.0040	-0.2279	-0.0040	0.7856	2.7856	Dissipative	High
M05	11	0.1559	-1.6932	-1.8490	63.3036	-0.0292	-1.6731	-0.0292	0.6034	2.6034	Intermediate	Medium
M06	14	0.4116	-0.3260	-0.7376	73.8875	-0.0100	-0.5720	-0.0100	0.7359	2.7359	Dissipative	High
M07	14	0.1859	-1.4255	-1.6114	89.3609	-0.0180	-1.0331	-0.0180	0.6756	2.6756	Dissipative	Medium
M08	14	0.3652	-1.8341	-2.1993	79.7940	-0.0276	-1.5788	-0.0276	0.6132	2.6132	Intermediate	Medium
M09	18	0.6109	-1.5508	-2.1616	79.8872	-0.0271	-1.5500	-0.0271	0.6163	2.6163	Intermediate	Medium
M10	11	0.1491	-1.9694	-2.1185	81.2497	-0.0261	-1.4936	-0.0261	0.6224	2.6224	Intermediate	Medium
M11	15	0.3226	-1.8940	-2.2166	86.7798	-0.0255	-1.4632	-0.0255	0.6257	2.6257	Intermediate	Medium
M12	12	-0.7221	-1.9195	-1.1974	63.0631	-0.0190	-1.0877	-0.0190	0.6689	2.6689	Dissipative	Medium
M13	13	0.1028	-1.9774	-2.0802	88.0381	-0.0236	-1.3536	-0.0236	0.6378	2.6378	Intermediate	Medium
M14	14	0.3364	-1.0225	-1.3589	101.6706	-0.0134	-0.7657	-0.0134	0.7097	2.7097	Dissipative	Medium
M15	25	0.2869	-2.0649	-2.3518	115.0818	-0.0204	-1.1707	-0.0204	0.6590	2.6590	Intermediate	Medium
M16	13	-1.1239	-2.0679	-0.9440	124.7550	-0.0076	-0.4335	-0.0076	0.7554	2.7554	Dissipative	High
SS01	21	-0.0649	-0.0053	0.0597	49.9114	0.0012	0.0685	0.0012	0.8318	2.8318	Dissipative	Very high
SS02	22	0.4405	-0.2342	-0.6747	75.8633	-0.0089	-0.5095	-0.0089	0.7446	2.7446	Dissipative	High
SS03	22	0.4571	-0.4785	-0.9356	79.7614	-0.0117	-0.6720	-0.0117	0.7222	2.7222	Dissipative	Medium
SS04	34	0.6554	-0.7550	-1.4104	79.8464	-0.0177	-1.0120	-0.0177	0.6782	2.6782	Dissipative	Medium
SS05	24	1.0163	-0.9901	-2.0064	87.0557	-0.0230	-1.3203	-0.0230	0.6416	2.6416	Intermediate	Medium
SS06	20	0.7606	-0.7723	-1.5329	79.8028	-0.0192	-1.1005	-0.0192	0.6674	2.6674	Dissipative	Medium
SS07	22	0.5759	-1.7717	-2.3476	87.4379	-0.0268	-1.5380	-0.0268	0.6176	2.6176	Intermediate	Medium
SS08	18	0.6713	-1.9038	-2.5751	91.5427	-0.0281	-1.6113	-0.0281	0.6098	2.6098	Intermediate	Medium
SS09	12	0.5930	-2.0647	-2.6577	81.4959	-0.0326	-1.8678	-0.0326	0.5839	2.5839	Intermediate	Low
SS10	18	0.0084	-1.9523	-1.9608	76.3159	-0.0257	-1.4718	-0.0257	0.6247	2.6247	Intermediate	Medium
SS11	12	-0.0010	-1.9470	-1.9460	76.6304	-0.0254	-1.4547	-0.0254	0.6266	2.6266	Intermediate	Medium
SS12	12	0.2182	-1.8693	-2.0876	98.0544	-0.0213	-1.2196	-0.0213	0.6532	2.6532	Intermediate	Medium

SS13	12	0.2098	-1.6996	-1.9093	93.9683	-0.0203	-1.1640	-0.0203	0.6598	2.6598	Intermediate	Medium
SS14	12	0.2603	-2.2350	-2.4953	92.1657	-0.0271	-1.5508	-0.0271	0.6162	2.6162	Intermediate	Medium
SS15	21	0.4896	-1.9709	-2.4605	100.3285	-0.0245	-1.4049	-0.0245	0.6321	2.6321	Intermediate	Medium
SS16	7	0.3905	-0.4731	-0.8636	109.1864	-0.0079	-0.4532	-0.0079	0.7526	2.7526	Dissipative	High

3.3. Morphometric, morphodynamic, and metoceanographic parameters

The multivariate analysis of variance (MANOVA) was applied to test whether the two beach sectors adjacent to the Porto do Malhado, Praia M (north, n = 16) and Praia SS (south, n = 16), differ significantly in their morphodynamic structure. Eight parameters were included in the analysis: number of points per profile (N_points), elevation of the first point (H_first_m), elevation of the last point (H_last_m), total elevation change (dH_m), horizontal profile length (Hdist_m), beach-face slope (tan_beta), wave run-up (Wr_m), and strandline altitude (SA_m).

Assumption tests revealed violations of the parametric requirements. Box's M test indicated heterogeneous covariance matrices among groups (χ^2 = NaN; df = 36; $p < 0.001$), and Mardia's multivariate normality test showed severe non-normality for skewness ($\chi^2 = 206.63$; df = 120; $p < 0.001$), although kurtosis was acceptable ($z = -1.85$; $p = 0.065$). Despite these violations, the four multivariate statistics converged consistently: Wilks' Lambda = 0.769 ($F = 1.255$; $p = 0.313$), Pillai's Trace = 0.233 ($F = 1.263$; $p = 0.310$), Hotelling-Lawley Trace = 0.300 ($F = 1.249$; $p = 0.316$), and Roy's Greatest Root = 0.295 ($F = 1.228$; $p = 0.325$). No significant multivariate difference was detected between Praia M and Praia SS ($p > 0.05$ for all four statistics).

Univariate ANOVAs confirmed the absence of significant differences for every individual parameter. The highest F-values were observed for N_points ($F = 4.084$; $\eta^2 = 0.120$; $p = 0.052$) and H_first_m ($F = 4.110$; $\eta^2 = 0.121$; $p = 0.052$), both marginally above the 5% significance threshold but with moderate effect sizes. The remaining parameters showed negligible effect sizes ($\eta^2 \leq 0.030$) and non-significant p-values (H_last_m: $F = 0.933$; $p = 0.342$; dH_m: $F = 0.017$; $p = 0.898$; Hdist_m: $F = 0.109$; $p = 0.744$; tan_beta: $F = 0.145$; $p = 0.706$; Wr_m: $F = 0.140$; $p = 0.711$; SA_m: $F = 0.140$; $p = 0.711$). After Bonferroni correction for multiple comparisons, no variable remained significant.

These results indicate that the Porto do Malhado structure does not induce statistically significant morphodynamic differences between the northern (M) and southern (SS) beach sectors, at least for the parameters analyzed and given the available sample size (n = 16 per group). Both sectors show statistically similar slope, run-up, strandline altitude, and horizontal extent, suggesting a comparable response to the regional wave regime and the presence of port infrastructure. The main methodological limitations are violations of multivariate normality and limited statistical power, which restricts detection to large effects ($\eta^2 > 0.25$). Future studies should consider increasing the sample size or applying non-parametric alternatives such as PERMANOVA.

Tabela 3. Summary of covariance homogeneity and multivariate normality tests, multivariate analysis of variance (MANOVA), and univariate analyses of variance (ANOVA) comparing profile-level variables between Malhado (M) and São Sebastião (SS) beaches, Ilhéus, Bahia, Brazil. Each beach includes 16 profiles. MANOVA results are presented as approximate F statistics. n = sample size; df = degrees of freedom; η^2 = eta-squared effect size. Statistical significance was assessed at $\alpha = 0.05$.

Test	Statistic	Value	p_value	Conclusion
Sample size	n	M = 16; SS = 16		—
Box's M (covariance homogeneity)	chi^2	nan (df = 36)		Heterogeneous
Mardia skewness (normality)	chi^2	206.630 (df = 120)	0,0000	Non-normal
Mardia kurtosis (normality)	z	-1.848	0,0647	Normal
MANOVA – Wilks' lambda	F	1.255	0,3133	Not significant
MANOVA – Pillai's trace	F	1.263	0,3098	Not significant
MANOVA – Hotelling-Lawley trace	F	1.249	0,3160	Not significant
MANOVA – Roy's greatest root	F	1.228	0,3254	Not significant
ANOVA – N_points	F	4.084 ($\eta^2 = 0.120$)	0,0523	Not significant
ANOVA – H_first_m	F	4.110 ($\eta^2 = 0.121$)	0,0516	Not significant
ANOVA – H_last_m	F	0.933 ($\eta^2 = 0.030$)	0,3419	Not significant
ANOVA – dH_m	F	0.017 ($\eta^2 = 0.001$)	0,8983	Not significant
ANOVA – Hdist_m	F	0.109 ($\eta^2 = 0.004$)	0,7435	Not significant
ANOVA – tan_beta	F	0.145 ($\eta^2 = 0.005$)	0,7061	Not significant
ANOVA – Wr_m	F	0.140 ($\eta^2 = 0.005$)	0,7109	Not significant
ANOVA – SA_m	F	0.140 ($\eta^2 = 0.005$)	0,7109	Not significant

4. Discussion

4.1. Geodetic accuracy and the representation of beach morphology

Geodetic accuracy defines the uncertainty associated with mapped beach elevations and derived morphometric attributes. GNSS observation precision must be distinguished from DEM accuracy, which also

depends on vertical referencing, sampling geometry, and interpolation. Systematic components associated with height conversion can affect coastal altimetry, making receiver precision alone insufficient to establish surface reliability (Santos et al., 2013). A consistent geodetic reference is essential for comparing beach sectors and successive surveys. Incompatible reference systems may generate apparent morphological differences unrelated to sedimentary processes. Geodetic integration therefore supports the spatial and temporal comparability required for interpreting beach morphology (Ferreira et al., 2014).

Datum-based shoreline indicators represent the intersection of a reference elevation with the beach surface and must be distinguished from the instantaneous waterline, which varies with hydrodynamic conditions. This distinction is essential when comparing shoreline positions obtained through different methods (Boak and Turner, 2005). On gently sloping beaches, vertical uncertainty can translate into considerable horizontal uncertainty, complicating the interpretation of contour displacement. Accuracy assessments based on discrete checkpoints characterize sampled locations and should be interpreted according to their spatial coverage, since uncertainty may vary across the modeled surface. A single-survey DEM consequently establishes a baseline for subsequent morphological assessments. Detecting erosion or accretion requires repeated observations, consistent geodetic references, and explicit propagation of survey and model uncertainties. Change-detection thresholds are necessary to distinguish sediment redistribution from measurement variability (Wheaton et al., 2010).

4.2. Morphometric contrasts and spatial variability around Malhado Port

Interpret spatial contrasts between M and SS within a coastal system where shoreline orientation, wave transformation, and sediment availability interact. Along Bahia, coastline geometry and wave incidence regulate longshore transport (Bittencourt et al., 2000). Accordingly, different shoreline alignments around Malhado Port may produce local contrasts even under a shared offshore wave climate; this remains a hypothesis that requires nearshore observations.

Within-beach variability also limits interpretations based on sector-wide averages. Elevation and slope maps can identify localized features, but elevation ranges and isolated slope maxima do not quantify sediment storage or coastal stability. Beach-face slope depends partly on sediment size and swash processes (Bujan et al., 2019), so steeper surfaces cannot be attributed solely to stronger wave exposure or port effects. Coastal structures can alter circulation and sediment pathways, potentially generating spatially uneven responses (Franzen et al., 2021). The expected pattern of updrift accumulation and downdrift sediment deficit depends on transport direction, sediment bypassing, and local geometry. Consequently, the mapped contrasts support hypotheses about sediment redistribution around the port, while establishing their causes requires integrated sedimentological, hydrodynamic, and multitemporal morphological evidence.

4.3. Wave forcing, morphodynamic states, and estimated coastal exposure

Offshore wave data provide a regional forcing context, while nearshore exposure depends on wave transformation, bathymetry, and interactions with coastal structures. Consequently, modeled offshore conditions represent forcing inputs whose relationship with wave action at individual profiles requires local assessment (Castelle and Masselink, 2023). Morphodynamic states describe coupled morphological and hydrodynamic behavior. Interpretation of intermediate and dissipative conditions requires consideration of breaker characteristics, sediment fall velocity, and surf-zone organization; classifications based mainly on profile slope remain provisional (Wright and Short, 1984). Dissipative conditions can sustain energetic infragravity motions, so gentle slopes do not necessarily imply limited run-up (Stockdon et al., 2006).

Run-up estimates integrate wave setup and swash and remain conditional on empirical model assumptions and input quality. Their value for comparing beach sectors depends on consistent definitions of foreshore slope and wave conditions, complemented by local validation (Stockdon et al., 2006). Estimated strandline altitude combines run-up with tidal elevation, describing potential water reach under the adopted scenario. Classes defined relative to the sample mean and standard deviation indicate comparative exposure, without establishing flooding probabilities or return periods. A very-high class also cannot establish storm-surge exposure when the meteorological water-level contribution is not explicitly included. Assessing inundation susceptibility therefore requires comparing estimated water levels with beach topography in a common vertical reference.

4.4. Statistical comparison between beach sectors and limits of inference

Interpretation of the sector comparison depends on a valid multivariate model. Including both endpoint elevations and their difference, or run-up and strandline altitude calculated with a fixed tidal elevation, introduces linear dependencies by construction. Such redundancy can produce singular or numerically unstable covariance matrices, requiring removal of redundant response variables and reassessment of model assumptions (Rencher and Christensen, 2012). An undefined Box's M statistic cannot establish covariance heterogeneity, and agreement among MANOVA criteria does not resolve these structural problems.

Once model validity is established, non-significant tests indicate insufficient evidence of differences under the tested hypotheses; they do not establish morphodynamic equivalence. Equivalence requires predefined

limits for geomorphologically meaningful differences and suitable tests. Effect estimates and confidence intervals should accompany significance tests, while claims about minimum detectable effects require a formal power or sensitivity analysis (Lakens, 2017).

Spatial dependence among neighboring profiles should also be examined, since nominal sample size may overstate independent information. The number of survey points primarily describes sampling effort and should be interpreted separately from morphodynamic attributes. Moreover, profile replication does not replicate beaches or port interventions. Without suitable control sectors and temporal replication, comparisons describe the surveyed conditions but cannot attribute differences to the port or demonstrate that it had no influence (Underwood, 1994).

4.5. Coastal monitoring, management, and SDG

Coastal zones are vital socioeconomic interfaces facing escalating vulnerability to climate-driven hazards, sea-level rise, and anthropogenic interventions such as port infrastructure, jetties, and urban expansion. Systematic and high-precision coastal monitoring, particularly using geodetic technologies like GNSS/RTK and high-resolution Digital Elevation Models (DEMs), is essential to quantify morphometric changes, evaluate cross-shore exposure, and discern local sediment redistribution patterns from measurement noise. From a coastal management perspective, accurate morphological baselines and robust statistical frameworks give local authorities empirical criteria to assess coastal vulnerability without relying solely on long-term decadal series. This methodological integration directly supports the targets established in the 2030 Agenda for Sustainable Development (United Nations, 2020, 2015). In particular, it contributes to SDG 14 (Life Below Water), Target 14.2, which urges sustainable management and protection of marine and coastal ecosystems to avoid significant adverse impacts and strengthen coastal resilience. Complementarily, rigorous geodetic data and exposure models advance SDG 11 (Sustainable Cities and Communities), specifically Target 11.b, by informing risk-reduction planning in urbanized coastal settlements, and SDG 13 (Climate Action) via Target 13.1 by strengthening adaptive capacity to episodic wave forcing and extreme metoceanographic events.

5. Conclusions

This study presented a methodological framework that couples geodetic-grade GNSS/RTK positioning, high-resolution Digital Elevation Models (DEM), and numerical wave reanalysis to assess beach morphometry and hydrodynamic exposure in coastal sectors influenced by port infrastructure. Independent vertical quality control verified the cartographic fidelity and metric precision of the generated elevation models, confirming that rigorous vertical referencing is essential for establishing reliable topographic baselines in coastal studies.

Integrating offshore wave data with coastal morphometric attributes enabled the assessment of beach-face slopes, estimated wave run-up, and potential water-level exposure across the surveyed shorelines. Multivariate and univariate statistical comparisons showed that overall morphodynamic and cross-shore characteristics remained statistically comparable between the south sector and the north of the port structure, indicating that cross-sectional beach geometry responded homogeneously under the observed modal oceanographic forcing.

These findings suggest that, within the spatial and temporal scope of a single survey campaign, the maritime structure does not produce pronounced cross-shore morphodynamic differentiation. However, identifying sediment-transport obstruction, longshore asymmetry, or localized deficits requires ongoing multitemporal monitoring, nearshore hydrodynamic characterization, and sedimentological tracking. Ultimately, the implemented geodetic and analytical workflow provides an objective, repeatable diagnostic tool to support shoreline management, risk reduction, and coastal planning, directly advancing the targets of Sustainable Development Goal (SDG) 14 (Target 14.2) for the protection of coastal ecosystems, while complementarily contributing to SDG 11 (Target 11.b) and SDG 13 (Target 13.1) by fostering urban shoreline resilience and adaptive capacity to metocean hazards.

6. References

Andrade, T.S. de, Sousa, P.H.G. de O., Siegle, E., 2019. Vulnerability to beach erosion based on a coastal processes approach. Applied Geography 102, 12–19. https://doi.org/10.1016/j.apgeog.2018.11.003

Bittencourt, A.C. da S.P., Dominguez, J.M.L., Martin, L., Silva, I.R., 2005. Longshore transport on the northeastern Brazilian coast and implications to the location of large scale accumulative and erosive zones: An overview. Mar. Geol. 219, 219–234. https://doi.org/10.1016/j.margeo.2005.06.006

Bittencourt, A.C. da S.P., Dominguez, J.M.L., Martin, L., Silva, I.R., 2000. Patterns of sediment dispersion coastwise the State of Bahia - Brazil. An. Acad. Bras. Cienc. 72, 271–287. https://doi.org/10.1590/S0001-37652000000200012

Boak, E.H., Turner, I.L., 2005. Shoreline definition and detection: A review. J. Coast. Res. 21, 688–703. https://doi.org/10.2112/03-0071.1

Bujan, N., Cox, R., Masselink, G., 2019. From fine sand to boulders: Examining the relationship between beach-face slope and sediment size. Mar. Geol. 417, 106012. https://doi.org/https://doi.org/10.1016/j.margeo.2019.106012

Cabral, F.T. de O., 2025. Uso das geotecnologias no estudo de erosão costeira: monitoramento multitemporal da variação da linha de costa nas praias de Gaibú e Suape, subsídio para reconstrução das áreas atingidas por erosão à gestão costeira, diante das mudanças climáticas, PE – Brasil. Revista Brasileira de Geografia Física 18, 3239–3268. https://doi.org/10.26848/rbgf.v18.4.p3239-3268

Calliari, L.J., Muehc, D., Hoefel, F.G., Toldo Jr., E., 2003. Morfodinâmica praial: uma breve revisão. Revista Brasileira de Oceanografia 51, 63–78. https://doi.org/10.1590/s1413-77392003000100007

Castelle, B., Masselink, G., 2023. Morphodynamics of wave-dominated beaches. Cambridge Prisms: Coastal Futures 1, e1. https://doi.org/10.1017/cft.2022.2

Cooley, S., Schoeman, D.S., Bopp, L., Boyd, P., Donner, S., Ito, S.-I., Kiessling, W., Martinetto, P., Ojea, E., Racault, M.-F., Rost, B., Skern-Mauritzen, M., 2022. Oceans and Coastal Ecosystems and Their Services, in: Pörtner, H.-O., Roberts, D.C., Tignor, M., Poloczanska, E.S., Mintenbeck, K., Alegría, A., Craig, M., Langsdorf, S., Löschke, S., Möller, V., Okem, A., Rama, B. (Eds.), Climate Change 2022: Impacts, Adaptation and Vulnerability. Cambridge University Press, Cambridge, pp. 379–550. https://doi.org/10.1017/9781009325844.005

Ferreira, A.T., Amaro, V.E., Santos, M.S.T., 2014. Geodésia aplicada à integração de dados topográficos e batimétricos na caracterização de superfícies de praia. Revista Brasileira de Cartografia 66.

Ferreira, A.T. da S., Amaro, V.E., Santos, M.S.T., 2014. Geodésia aplicada à integração de dados topográficos e batimétricos na caracterização de superfícies de praia. Revista Brasileira de Cartografia 66, 167–184.

Ferreira, A.T. da S., Amaro, V.E., Santos, M.S.T., Marcelino, A.M.T., Almeida, L.R. de, Ribeiro, M.C.H., 2019. Método de identificação de áreas de inundação costeira por sobrelevação do nível do mar a eventos extremos, em escala local, in: Sistema de Modelagem Costeira Do Brasil: Estudos de Caso. UFSC, p. 411.

Ferreira, A.T. da S., de Oliveira, R.C., Ribeiro, M.C.H., de Freitas Sousa, P.S., de Paula Miranda, L., de Oliveira Folharini, S., Siegle, E., 2025a. Microplastic Deposit Predictions on Sandy Beaches by Geotechnologies and Machine Learning Models. Coasts 5, 4. https://doi.org/10.3390/coasts5010004

Ferreira, A.T. da S., Oliveira, R.C. de, Ribeiro, M.C.H., Grohmann, C.H., Siegle, E., 2023. Coastal Dynamics Analysis Based on Orbital Remote Sensing Big Data and Multivariate Statistical Models. Coasts 3, 160–174. https://doi.org/10.3390/coasts3030010

Ferreira, A.T. da S., Oliveira, R.C. de, Siegle, E., Ribeiro, M.C.H., Esteves, L.S., Kuznetsova, M., Dipold, J., Freitas, A.Z. de, Wetter, N.U., 2025b. Microplastic Deposits Prediction on Urban Sandy Beaches: Integrating Remote Sensing, GNSS Positioning, μ-Raman Spectroscopy, and Machine Learning Models. Microplastics 4, 12. https://doi.org/10.3390/microplastics4010012

Ferreira, A.T. da S., Santos, M.S.T., Fernandes, L.D.R., Ribeiro, M.C.H., 2016. Mapeamento Geomorfológico De Detalhe Para Delimitação De Áreas De Preservação Permanente (App) De Zonas Costeiras Em Atendimento Ao Cadastro Ambiental Rural (Car). Revista Brasileira de Geomorfologia 17. https://doi.org/10.20502/rbg.v17i4.671

Ferreira, A.T. da S., Siegle, E., Ribeiro, M.C.H., Santos, M.S.T., Grohmann, C.H., 2021. The dynamics of plastic pellets on sandy beaches: a new methodological approach. Mar. Environ. Res. 163, 105219. https://doi.org/10.1016/j.marenvres.2020.105219

Ferreira, A.T. da S., Wetter, N.U., Ribeiro, M.C.H., Esteves, L.S., Dias, A.J.G., Grohmann, C.H., Kuznetsova, M., Freitas, A.Z. de, Oliveira, R.C. de, Siegle, E., 2024. Recognizing microplastic deposits on sandy beaches by altimetric positioning, μ-Raman spectroscopy and multivariate statistical models. Mar. Pollut. Bull. 209, 117025. https://doi.org/10.1016/j.marpolbul.2024.117025

Ferreira, A.T.S., Grohmann, C.H., Ribeiro, M.C.H., Santos, M.S.T., de Oliveira, R.C., Siegle, E., 2024. Beach surface model construction: A strategy approach with structure from motion - multi-view stereo. MethodsX 12, 102694. https://doi.org/10.1016/j.mex.2024.102694

Franzen, M., Siegle, E., Sottolichio, A., Fernandes, E.H.L., 2026. Influence of Long Jetties on Coastal and Estuarine Hydro-Sedimentological Patterns in a Microtidal Region: Potential for Mud Deposit Formation. Coasts 6, 17. https://doi.org/10.3390/coasts6020017

Franzen, M.O., Fernandes, E.H.L., Siegle, E., 2021. Impacts of coastal structures on hydro-morphodynamic patterns and guidelines towards sustainable coastal development: A case studies review. Reg. Stud. Mar. Sci. 44, 101800. https://doi.org/10.1016/j.rsma.2021.101800

Gallerano, F., Palleschi, F., Iele, B., 2020. Numerical Study over the Effects of a Designed Submerged Breakwater on the Coastal Sediment Transport in the Pescara Harbour (Italy). J. Mar. Sci. Eng. 8, 487. https://doi.org/10.3390/jmse8070487

Gaya, J., Alves, T., Córdova Júnior, L., Leandro dos Santos, M., 2022. Dinâmica da orla da Praia de Navegantes (Santa Catarina, Brasil) através do sensoriamento remoto. Revista de Gestão Costeira Integrada 22, 249–261. https://doi.org/10.5894/rgci-n456

Guerra, F.C., da Silva Ferreira, A.T., da Silva, G.P., de Oliveira, R.C., Gonçalves, R.D., 2025. Dinâmica demográfica e erosão costeira no litoral centro de Sergipe: Uma análise integrada sob a perspectiva da teoria geral dos sistemas. Scientia Plena 21.

Halaj, M., Kačmařík, M., 2022. Performance Assessment of Kinematic GNSS Positioning with Smartphones Based on Post-Processing of Raw Observations. GeoScience Engineering 68, 178–194. https://doi.org/10.35180/gse-2022-0080

Hofmann-Wellenhof, B., Lichtenegger, H., Wasle, E., 2008. GNSS — Global Navigation Satellite Systems, 1st ed. Springer Vienna, Vienna. https://doi.org/10.1007/978-3-211-73017-1

Holthuijsen, L.H., 2007. Waves in Oceanic and Coastal Waters. Cambridge University Press. https://doi.org/10.1017/CBO9780511618536

Krueger, C.P., Oliveira Junior, P.S. de, Garnés, S.J. dos A., Alves, D.B.M., Euriques, J.F., 2020. Posicionamento GNSS em Tempo Real: Evolução, Aplicações Práticas e Perspectivas para o Futuro. Revista Brasileira de Cartografia 72, 1359–1379. https://doi.org/10.14393/rbcv72nespecial50anos-56620

Lakens, D., 2017. Equivalence Tests. Soc. Psychol. Personal. Sci. 8, 355–362. https://doi.org/10.1177/1948550617697177

Lobo, M.S., Santos, B.S.S., Lavenère-Wanderley, A.A.D.O., 2017. Análise Estatística Anual e Mensal das Ondas Atuantes na Costa de Ilhéus (Bahia) Baseada na Reanálise de Série Temporal de 31 Anos do Modelo de Ondas WAVEWATCH III. Geography Department University of Sao Paulo 67. https://doi.org/10.11606/rdg.v0ispe.132752

Mentaschi, L., Vousdoukas, M.I., Pekel, J.-F., Voukouvalas, E., Feyen, L., 2018. Global long-term observations of coastal erosion and accretion. Sci. Rep. 8, 12876. https://doi.org/10.1038/s41598-018-30904-w

Monico, J.F.G., 2008. Posicionamento pelo GNSS: descrição, fundamentos e aplicações, São Paulo. Editora UNESP, São Paulo.

Pianca, C., Mazzini, P.L.F., Siegle, E., 2010. Brazilian offshore wave climate based on NWW3 reanalysis. Braz. J. Oceanogr. 58, 53–70. https://doi.org/10.1590/s1679-87592010000100006

Rencher, A.C., Christensen, W.F., 2012. Methods of Multivariate Analysis. Wiley. https://doi.org/10.1002/9781118391686

Saengsupavanich, C., Rif'atin, H.Q., Magdalena, I., Ariffin, E.H., 2024. A systematic review of jetty-induced downdrift coastal erosion management. Reg. Stud. Mar. Sci. 74, 103523. https://doi.org/10.1016/j.rsma.2024.103523

Santos, F.G. dos, 2016. A Baía do Pontal – Ilhéus: relações do porto com a cidade (1911-1971). Revista Crítica Histórica 7. https://doi.org/10.28998/rchvl7n13.2016.0002

Santos, M.S.T., Amaro, V.E., 2013. Dinâmica sazonal de processos costeiros e estuarinos em sistema de praias arenosas e ilhas barreira no Nordeste do Brasil. Revista Brasileira de Geomorfologia 14. https://doi.org/10.20502/rbg.v14i2.298

Santos, M.S.T., Amaro, V.E., Ferreira, A.T. da S., Santos, A.L.S. dos, 2013. Altimetria GNSS de precisão aplicada ao monitoramento da dinâmica sedimentar costeira de curta duração em escala regional. Boletim de Ciências Geodésicas 19, 624–638. https://doi.org/10.1590/S1982-21702013000400007

Short, A.D., 1999. Handbook of beach and shoreface morphodynamics. John Wiley & Sons, USA.

Sofia, G., Eltner, A., Nikolopoulos, E., Crosby, C., 2019. Leading Progress in Digital Terrain Analysis and Modeling. ISPRS Int. J. Geoinf. 8, 372. https://doi.org/10.3390/ijgi8090372

Stockdon, H.F., Holman, R.A., Howd, P.A., Sallenger Jr., A.H., 2006. Empirical parameterization of setup, swash, and runup. Coastal Engineering 53, 573–588. https://doi.org/10.1016/j.coastaleng.2005.12.005

Tang, J., Lyu, Y., Shen, Y., Zhang, M., Su, M., 2017. Numerical study on influences of breakwater layout on coastal waves, wave-induced currents, sediment transport and beach morphological evolution. Ocean Engineering 141, 375–387. https://doi.org/10.1016/j.oceaneng.2017.06.042

Taveira-Pinto, F., Rosa-Santos, P., Fazeres-Ferradosa, T., Bento, A.M., Carrasco, A.R., 2022. Dinâmica sedimentar, erosão costeira e gestão portuária. Revista de Gestão Costeira Integrada 22, 245–248. https://doi.org/10.5894/rgci-n562

Timm, N.H., 2002. Multivariate Regression Models, in: Timm, Neil H (Ed.), Applied Multivariate Analysis. Springer New York, New York, NY, pp. 185–309. https://doi.org/10.1007/978-0-387-22771-9_4

Tolman, H., Balasubramaniyan, B., Burroughs, L., Chalikov, D., Chao, Y., Chen, H., Gerald, V., 2002. Development and Implementation of Wind-Generated Ocean Surface Wave Modelsat NCEP. Weather and Forecasting - WEATHER FORECAST 17, 311–333. https://doi.org/10.1175/1520-0434(2002)017<0311:DAIOWG>2.0.CO;2

Uda, T., Yamamoto, K., 1994. Beach Changes Caused by Obstruction of Longshore Sand Transport: An Example of the Hidaka Coast in Hokkaido. Coastal Engineering in Japan 37, 87–106. https://doi.org/10.1080/05785634.1994.11924588

Underwood, A.J., 1994. On Beyond BACI: Sampling Designs that Might Reliably Detect Environmental Disturbances. Ecological Applications 4, 3–15. https://doi.org/10.2307/1942110

United Nations, 2020. The Sustainable Development Goals Report 2020. United Nations; 2020.

United Nations, 2015. Transforming our world: the 2030 Agenda for Sustainable Development, United Nations, Department of Economic and Social Affairs. New York.

Wheaton, J.M., Brasington, J., Darby, S.E., Sear, D.A., 2010. Accounting for uncertainty in DEMs from repeat topographic surveys: improved sediment budgets. Earth Surf. Process. Landf. 35, 136–156. https://doi.org/10.1002/esp.1886

Wright, L.D., Short, A.D., 1984. Morphodynamic variability of surf zones and beaches: A synthesis. Mar. Geol. 56, 93–118. https://doi.org/10.1016/0025-3227(84)90008-2